A DSP EMBEDDED OPTICAL NAVIGATION SYSTEM

A Thesis

by

KIRAN KUMAR GUNNAM

Submitted to the Office of Graduate Studies of
Texas A&M University
in partial fulfillment of the requirements for the degree of

MASTER OF SCIENCE

May 2003

Major Subject: Electrical Engineering

A DSP EMBEDDED OPTICAL NAVIGATION SYSTEM

A Thesis

by

KIRAN KUMAR GUNNAM

Submitted to Texas A&M University
in partial fulfillment of the requirements
for the degree of

MASTER OF SCIENCE

Approved as to style and content by:

Nasser Kehtarnavaz (Co-Chair of Committee)	John L. Junkins (Co-Chair of Committee)
Krishna Narayanan (Member)	Edward R. Dougherty (Member)
Chanan Singh (Head of Department)	

May 2003

Major Subject: Electrical Engineering

ABSTRACT

A DSP Embedded Optical Navigation System. (May 2003)

Kiran Kumar Gunnam, B.Tech., Jawaharlal Nehru Technological University

Co-Chairs of Advisory Committee: Dr. John L. Junkins
Dr. Nasser Kehtarnavaz

Spacecraft missions such as spacecraft docking and formation flying require high precision relative position and attitude data. Although Global Positioining Systems can provide this capability near the earth, deep space missions require the use of alternative technologies. One such technology is the vision-based navigation (VISNAV) sensor system developed at Texas A&M University. VISNAV comprises an electro-optical sensor combined with light sources or beacons. This patented sensor has an analog detector in the focal plane with a rise time of a few microseconds. Accuracies better than one part in 2000 of the field of view have been obtained. This research presents a new approach involving simultaneous activation of beacons with frequency division multiplexing as part of the VISNAV sensor system. In addition, it discusses the synchronous demodulation process using digital heterodyning and decimating filter banks on a low-power fixed point DSP, which improves the accuracy of the sensor measurements and the reliability of the system. This research also presents an optimal and computationally efficient six-degree-of-freedom estimation algorithm using a new measurement model based on the attitude representation of Modified Rodrigues Parameters.

To

My Parents , Brother and Sister

ACKNOWLEDGMENTS

I would like to express my gratitude for Dr. Declan Hughes, Research Engineer, NASA Commercial Space Center for Engineering who supervised my research work performed in the VISNAV Lab. He provided invaluble mentoring and direction for my work by explaining the key concepts of the sensor and the ways to explore further. I am thankful for his help encompassing the entire duration of the project in a wide spectrum of issues ranging from concepts and algorithms to hardware and software issues; without this help my thesis would not have been possible.

I would like to express my gratitude for Dr. John Junkins, my advisor for giving me the chance to work on this exciting spacecraft navigation project and guiding my research. I am thankful for him for teaching me the concepts in six degrees of freedom data estimation and providing the key insights necessary to pursue this research. I am thankful for his enthusiasim to discuss the problems in research and providing the direction in the weekly meetings and also when ever I approached him.

I would like to express my gratitude for Dr. Nasser Kehtarnavaz, my advisor for guiding my research and graduate studies.I am thankful for him for teaching me the advanced concepts in Digital Signal Processors and providing the key insights for the real time implemenation of the data estimation and signal processing algorithms. I am thankful for his time in shaping and refining my research. I am thankful for him in providing the direction and guidance in a number of academic and career issues.

I am thankful for Dr. John Valasek for giving me the chance to work with him for the aerial refueling project. I am thankful for Miss. Ju Young Du , PhD student in aerospace engineering with Dr.Junkins for providing me the analytical and simulation frame work of data estimation using modified rodrigues parameters. I am thankful for the other project members Mr.Roberto Alonso, Miss. Jennifer Kimmet and Mr. Srivatsan Thiruvengadam for their interaction and help in my work. I am also thankful for Dr.Mark Yeary for his friendly advice and interaction during my graduate studies.

I am thankful for Dr. Krishna Narayanan and Dr. Edward Dougherty for serving on my thesis committee and their time in reviewing in the thesis document.

I am thankful for Miss. Tammy Carda for her critical assistance in number of academic issues. I am thankful for Miss. Lisa Willingham for her administrative support and help. I am thankful for the staff and computing support in Dept. Electrical Eng and Dept. Aerospace Eng for their help. I am thankful for the staff in International Student Services for their help in practical training issues.

TABLE OF CONTENTS

Page

Page

LIST OF FIGURES

FIGURE Page

LIST OF TABLES

I. INTRODUCTION*

A. Six Degrees of Freedom Data Estimation and VISNAV Sensor

Several research efforts have been carried out in the field of six-degrees-of-freedom (6DOF) position and attitude estimation for rendezvous and proximity operations. The Vision based Navigation (VISNAV) sensor system developed at Texas A&M University [1] is aimed at achieving better accuracies in 6DOF estimation using a simpler yet more robust approach. It uses measurements from a Position Sensitive Diode (PSD) sensor to calculate 6DOF estimates of the sensor location and orientation. The PSD sensor generates four currents whose imbalances are linearly proportional to the azimuth and elevation of the light source with respect to the sensor. The individual currents, which depend on the intensity of the light, are kept nearly constant by using a feedback control of the light source output power. This is done to accommodate for variable received energy due to range dependence and other factors. By having four or more light sources (called beacons) in the target frame at known positions, the 6DOF data associated with the sensor are calculated. An electromagnetic signature is given to the beacon by modulating the beacon (an array of LEDs) at a distinct frequency to -

---

This thesis follows the style and format of *IEEE Sensors Journal*.

* Portions of this thesis are reprinted, with permission, from K.Gunnam, D.Hughes, J.Junkins, and N.Kehtarnavaz "A Vision-Based DSP Embedded Optical Navigation Sensor", *IEEE Sensors Journal*, vol.2, pp. 428-442,October 2002.

distinguish target energy from the ambient optical energy such as sunlight. The beacons are operated at a single frequency in Time Division Multiplexing (TDM) mode in the original VISNAV configuration. Demodulation of the sensor currents to recover the signals is done via analog circuitry in this configuration.

B. A New Configuration for VISNAV System

In the new configuration of VISNAV, different targets are operated simultaneously at different frequencies for identification purposes as done in Frequency Division Multiplexing (FDM). The advantage of using FDM is that it satisfies the implicit assumption of the 6DOF estimation that all the beacon measurements are taken at the same time. If the beacons are operated in TDM and the rate of change of 6DOF data is high, the estimates based on the measurements, even without considering the motion between successive measurements, will induce errors. These errors can be reduced by the FDM approach. In the case of TDM, the lowpass filter after the demodulation needs to have a passband of about $N \times 100Hz$ (N is the number of beacons, 100 Hz is the 6DOF data update rate), where as in FDM, it needs to be only $100Hz$ resulting in an N factor improvement in the signal to noise power ratio (SNR) of the beacon currents. To achieve the same N factor improvement in the SNR in the TDM mode, the peak power of the LED beacons has to be increased by N so that it will consume the same average power as in the FDM mode. However, this may not be a viable solution since a large number of LEDs is required because of the increased peak power requirements. Here the beacon channel separation and

demodulation are done on a fixed point Digital Signal Processor (DSP) Texas Instruments TMS320C55x (C55x) [2] using digital down conversion, synchronous detection and multi-rate signal processing techniques. The demodulated sensor currents due to each beacon are communicated to a floating point DSP Texas Instruments TMS320VC33 (VC33) [2] for the subsequent navigation solution by the use of colinearity equations and a Gaussian Least Squares Differential Correction (GLSDC) algorithm. There are several advantages in performing the demodulation in the digital domain. The new configuration of the VISNAV sensor system is easily reprogrammed and insensitive to temperature variations and aging effects. It is also easily scaled up to 16 beacons with slight modifications in the software.

The experimental results show that a beacon's line-of-sight vector can be determined with an accuracy of approximately one part in 2000 of the sensor field of view (90 degree cone) angle at a distance of 30m with an update rate of 100Hz. 6DOF navigation accuracies of less than 2 mm in translation estimates and less than 0.01 degrees in orientation estimates at rendezvous, updated at 100Hz, are routinely possible by solving the colinearity equations for four or more beacons. Processing of these 6DOF estimates with a Kalman filter permits estimation of the relative motion velocity and acceleration with heretofore unachievable accuracy. Autonomous rendezvous and docking operations are thus enabled as a direct consequence of precise, reliable, high bandwidth proximity navigation. The VISNAV sensor system has several advantages such as small sensor size, wide sensor field of view, no time-consuming image

processing, relatively simple electronics and very small errors in 6DOF data of the order of 2mm in position estimates and 0.01 degrees in attitude estimates at rendezvous.

C. Related Work

There is considerable research being done in the field of 6DOF estimation for rendezvous and proximity operations [3-9]. In 1999, NASA developed and tested a Video Guidance Sensor [6,7] which used a CCD based video camera to capture the images of a laser illuminated passive target and an on board computer to process the images in order to determine the relative position and attitude of the target. This system operates from a 1.5-meter range out 110-meter range, with a field–of-view of 16 x 21 degrees and has an update rate of 5 Hz. At rendezvous the displacement errors will be around 3 mm in magnitude and orientation errors will be around 0.3 degrees in magnitude. Though this system provides good 6DOF estimates, the 6DOF data extraction from image data requires complex image processing which puts limits on the update rate. Because of the passive target and the complex sensor hardware the total system power consumption will be around 400 watts, which is a stress on limited on board power resources. A similar system, based on target pattern recognition, was developed by S. D. Lender et al [8]. This system also has the same type of advantages and disadvantages as the Video Guidance Sensor.

Another popular 6DOF system is based on differential GPS that provides good accuracies for mid ranges. The National Space Development Agency of Japan used this

relative GPS technique on an Engineering Test Vehicle VII (ETS-VII) in 1997 [9]. In this relative GPS, the GPS measurements of a passive target are communicated to the chase craft using a RF link in real time. The active chase craft applies a navigation filter to the GPS measurements from both the chase craft and the target craft to determine 6DOF estimates. The systems based on differential GPS will be limited by Selective Availability of the satellites, Geometric Dilution of Precision, Ephemeris errors, Multi-path errors, Satellite Clock errors, receiver errors etc. These systems will provide good 6DOF estimates with position errors of the order of sub centimeters and attitude errors of the order of 1 to 2 degrees. Although by using Carrier phase measurement for GPS the errors due to multi path and other factors can be reduced, all the errors cannot be eliminated and these GPS based systems become complicated.

There is another class of 6DOF system, which is based on star pattern recognition. One such example is StarNav developed by Junkins et al [10]. Though these types of systems give 6DOF estimates with good accuracy for spacecraft navigation,they are not intended for provding the data for rendezous operations.

Other sensing systems based on lasers, Charge Couple Devices (CCD) and high-speed cameras require complex image processing and target identification with associated occasional failures. These systems have typically slower update rates limited by frame rates and time-consuming image processing algorithms.

D. Applications

The VISNAV sensor has lot of applications where precision 6DOF data is necessary. Some of the primary applications include spacecraft docking/maneuvering, formation flying, flight aircraft refueling operations, vertical takeoff and landing navigation for aircraft, human body motion capture, and robot arm end effector position/attitude sensing [1]. Different applications of VISNAV such as formation flying and aerial refueling are discussed in [9], [10] and more information can be found at the VISNAV Lab website [11]. The photographs of the sensor and active beacons of VISNAV are shown in Figs. 1 and 2, respectively. Figure 3 illustrates a spacecraft docking scenario using the VISNAV sensor.

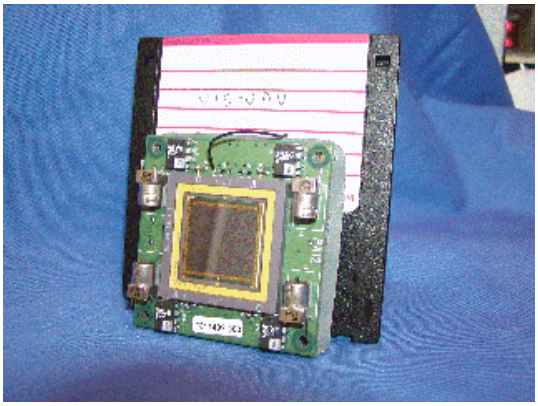

Fig. 1. VISNAV PSD and pre-amplifiers.

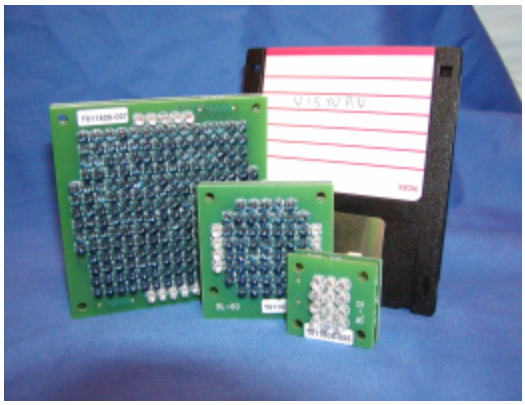

Fig. 2. Active beacons (of three different sizes).

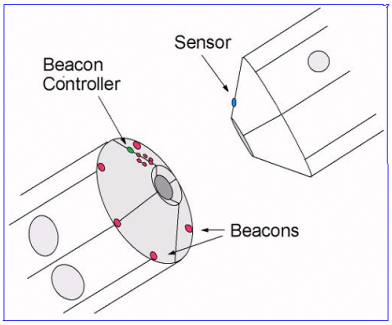

Fig. 3. Spacecraft docking using the VISNAV sensor system. Active beacons are fixed on one spacecraft while the PSD sensor is fixed on another spacecraft. Some beacons are placed near the docking point and some are placed wide apart to provide a wide range of field of view.

II. SENSOR DATA ESTIMATION

A.Sensor Description

Position Sensing Diode (PSD) is a single substrate photodiode capable of finding or locating a light beam within a defined sensing area. One class of PSDs is the area PSD that can measure the two-dimensional beam position. When photons reach the PSD sensor, electric currents are generated that flow through its four terminals, each terminal being on one side of the rectangular PSD. The closer the incident light is to a particular terminal, the larger the current flowing through that terminal. Comparisons of these four currents then determine the centroid location of the incident light from the target light source (beacon).

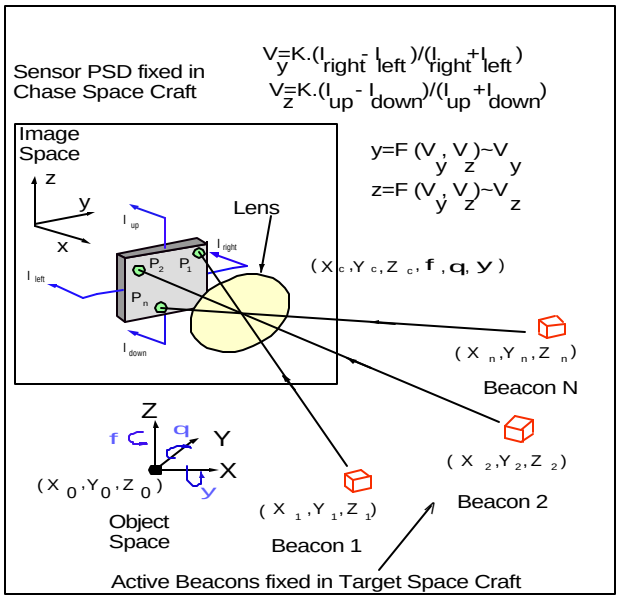

Fig. 4. Sensor geometry.

As indicated in Fig. 4, the following unitless normalized voltages are defined,

$$V_y = K\frac{I_{right} - I_{left}}{I_{right} + I_{left}}\ , \tag{1}$$

and

$$V_z = K\frac{I_{up} - I_{down}}{I_{up} + I_{down}} \tag{2}$$

where K is a constant of value 1. V_y corresponds to the angle that the incident light beam makes about the image space y-axis. Similarly V_z corresponds to the angle that the incident light beam makes about the image space z-axis.

However, there are several problems in this simple approach that get resolved by the VISNAV sensor [1]. Often there exists a large amount of ambient light at short wavelengths and low frequencies due to the sun, its reflections, incandescent or discharge tube lights, LCD and cathode ray tube displays, etc. In many cases this ambient energy swamps the relatively small beacon signal and the PSD centroid data then mostly correspond to this unwanted background light. In order for the beacon light to dominate the PSD response, all energy at shorter wavelengths than those of the beacon are significantly reduced by an optical color filter. Furthermore, a sinusoidal carrier of approximately 40KHz frequency is applied to modulate each beacon LED drive current. The resulting induced PSD signal currents then vary sinusoidally at approximately the same frequency (depending on the position and attitude of the PSD sensor with respect to the beacon) and are demodulated to recover the currents that are

proportional to the beacon light centroid. This modulation/demodulation scheme leads to a high degree of insensitivity to variations in ambient lighting conditions, and it is thus the key to making the PSD sensing approach practical.

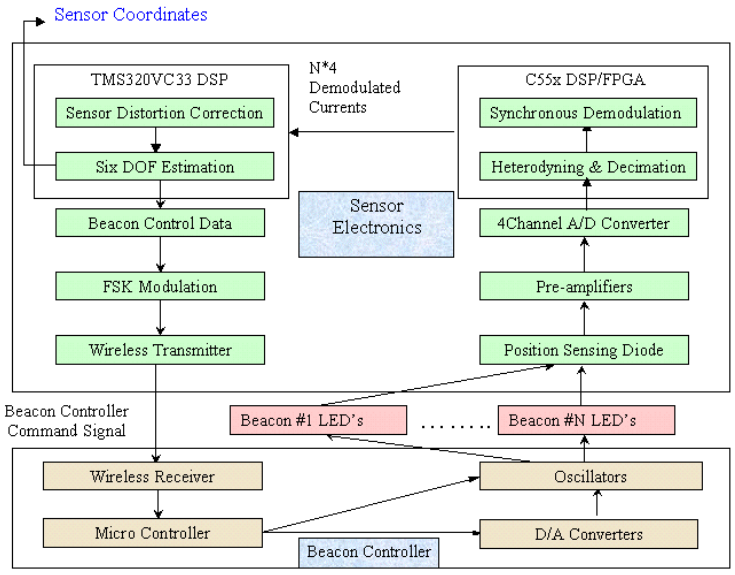

Fig. 5. Signal processing schematic.

The DSP unit of the sensor controls the intensity of beacon lights by sending control data to the beacon controller via a radio data link to achieve the power modulation feature [1], refer to Fig. 5. The control data contains N bytes where each byte is an integer approximation to the average PSD current level induced by each beacon during the most recent measurement. If a beacon output power level is too high,

one or more of the four PSD signal transimpedance amplifiers may saturate and the incident light centroid cannot be accurately determined. In order to prevent this, feedback control is used to hold the beacon light intensity at a level that results in a maximum PSD current at approximately 70% of the transimpedance amplifier input saturation level; this is also important for optimizing the system signal-to-noise ratio. The beacon controller compares the "maximum PSD current" byte to the beacon control intensity to determine whether this intensity should be increased, decreased, or left unchanged next time it is activated. If there are N beacons, only those beacons which are in the near field of view can be activated as long as at least four beacons are turned on. This power modulation feature automatically accommodates for variable received energy due to range variations, viewing angle dependence, atmospheric conditions, and off-nominal beacon performance [1].

For solving a 6DOF estimation problem, it is required to have PSD measurements for at least four beacons, which are (ideally) arranged in a non-planar surface [1]. In practical applications, more beacons may be used for the sake of robustness and to better cover the sensor field of view (FOV) at different beacon/sensor separations. These beacons may be selected from a larger set of beacons based on a figure of merit such as the magnitude of the largest PSD signal current. In the present configuration of VISNAV, the beacons are operated in the TDM mode. Operating all beacons simultaneously at different frequencies (i.e. FDM) has advantages in terms of higher SNRs for the PSD measurements and more accurate 6DOF estimates.

B. Modulation and Frequency Division Multiplexing

The PSDs are relatively fast compared to even high-speed cameras, having rise times of about five microseconds. This permits light sources to be structured in the frequency domain and utilization of radar-like signal processing methods to discriminate target energy in the presence of highly cluttered ambient optical scenes. If there is a single beacon excited by a sinusoidal oscillator operating at a frequency f_c, the emitted light induces sinusoidal currents in the PSD with the frequency f_c at the four terminals of the PSD sensor. Therefore, all the four currents can be processed in a similar fashion to estimate the amplitudes of the carrier waveforms. The amplitudes of these currents are related to the azimuth and elevation of the light source with respect to the image coordinate frame. If the PSD has a relative motion with respect to the beacon, the current envelopes are modulated by that relative motion and this modulation is analogous to Amplitude Modulation (AM). Thus, the currents can be written as follows:

$$I_k(t) = (A_k.Cos(2.pi.f_c.t).(1+m_k(t))) + n_k, \quad (3)$$

where $k = 1,2,3,4$ and it corresponds to the terminal number of the PSD, A_k is the amplitude of the current waveform generated at the k^{th} terminal of the PSD by the beacon that is fixed with respect to the PSD sensor. The function $m_k(t)$ denotes the signal envelope variation induced by the relative movement of the sensor. This bandwidth limited signal is assumed to be dominated by less than 10Hz frequencies.

The noise term n_k is considered to be white Gaussian with a maximum frequency of f_{MAX} where $f_c < f_{MAX}$, $f_{MAX} = f_s / 2$, with f_s indicating the sampling frequency.

If there are multiple beacons operating at different frequencies, then the PSD terminal currents consist of current components at those frequencies, and can be written as follows:

$$I_k(t) = \sum_{j=1}^{N} (A_{j,k}.Cos(2.pi.f_j.t).(1 + m_{j,k}(t))) + n_{j,k} \quad (4)$$

where N is the number of beacons and it should be greater than four for solving the 6DOF inverse problem, $A_{j,k}$ is the peak amplitude of the current generated at the k^{th} terminal of the PSD corresponding to a light beam from the j^{th} beacon driven by a sinusoidal oscillator of frequency f_j while the beacon is fixed with respect to the PSD sensor, $m_{j,k}(t)$ is the signal due to the relative movement of the sensor with respect to the j^{th} beacon, and $n_{j,k}$ is the noise component due to the j^{th} beacon at the k^{th} terminal. It is required to demodulate the above composite currents in real-time for $N*4$ channels. The components to be recovered can thus be modeled as

$$r_{j,k}(t) = A_{j,k}(1 + m_{j,k}(t)),\ j = 1,..,N; k = 1,...,4 \quad (5)$$

It is worth pointing out that the normalized voltages, which are proportional to azimuth and elevation of the j^{th} beacon with respect to the image coordinate frame, are obtained from the following relation, similar to (1):

$$V_{y,j} = K\frac{r_{j,1} - r_{j,2}}{r_{j,1} + r_{j,2}}\ , \tag{6}$$

$$\text{and } V_{z,j} = K\frac{r_{j,3} - r_{j,4}}{r_{j,3} + r_{j,4}} \tag{7}$$

The selection of frequencies for the beacons is based on several factors. The beacon frequency should ideally be above 20 KHz in order to distinguish it from lower frequency background ambient light that might include extraneous lighting sources. If the beacon frequency is too high, the PSD/preamplifier noise will be greater. For practical purposes the beacon frequency is selected to be near 40 KHz. The separation between the beacon frequencies depends on the bandwidth of the beacon signal. The bandwidth is proportional to the relative motion of the sensor with respect to the beacons and the required 6DOF data update rate. The VISNAV sensor system is designed for applications with movement frequency components mostly limited to 10 Hz and for the 6DOF data update rate of 100 Hz. The 6DOF update rate is set to 100 Hz (10*10Hz) in order to allow feedback control at up to 10Hz, and to provide relatively accurate monitoring of spacecraft acceleration profiles during thrusting. Accounting for the two sidebands resulting from the modulation of the beacon signal, the beacon channel bandwidth is chosen to be around 200 Hz. In order to achieve an acceptable adjacent beacon channel rejection with reasonable filtering requirements, the guard band is set at 300 Hz. For the test configuration of 8 beacons, the beacon carrier frequencies are chosen to start from 48.5Khz with an inter channel separation of

500 Hz. When the sensor faces sunlight, extra noise of about 5 to 10 times the usual noise level is expected. In this case, de-focusing of the lens helps to minimize the maximum energy density at the silicon surface of the PSD sensor preventing damage to the sensor. Accelerometers can be added for high frequency state information if noise is considered too excessive in some applications. Beacon intensities can also be increased to obtain greater signal strength.

C. Demodulation Approaches

Considering that it is needed to determine the amplitude of the sinusoidal signal and the associated signal due to the relative movement of the sensor, an approach similar to AM demodulation is used here. The main difference, however, is that we are also interested in the carrier amplitude. Although analog circuits can be used to perform the channel separation and demodulation, the DSP-based approach provides a more cost-effective solution with a higher degree of reliability, programmability and scalability.

In the foregoing discussion, it is shown that for real-time implementation on a DSP processor, straight envelope detection is not feasible and the use of multi-rate signal processing (refer to Fig.6 and Fig.7 for the method used) can overcome this limitation. The PSD sensor generates four currents and a four channel synchronous Analog to Digital Converter (ADC) samples these four currents. Each current contains the frequency components from around 48.25 KHz to 52.25 KHz. Also, each current contains low frequency components whose strength depends on the intensity of

ambient cluster and preamplifier noise components, which are modeled as additive white Gaussian noise as high as 105 KHz depending on the bandwidth of the preamplifier. Since the signal bandwidth is only 2KHz (48.25-52.25 KHz), bandpass filtering can be performed requiring a sampling frequency of only 4 KHz (2*2KHz). But this demands a complex analog bandpass filter before the ADC to achieve the required attenuation in the stopband. Such a filter requires many poles to achieve the stringent attenuation requirements and also mechanisms for tuning, such as switched capacitors to have stable bandwidth. Therefore, this approach is rather complex and costly when done in the analog-front-end. Hence, an alternative approach based on multi-rate signal processing is deployed here to overcome the complexity problem.

The sampling frequency of the ADC is chosen to be 210 KHz, which is four times the anticipated maximum frequency component of interest or 52.5 KHz. This sampling frequency satisfies the Nyquist sampling rate for frequencies up to 105 KHz, noting that the requirements on the anti-aliasing filter is very moderate. Four preamplifiers with unity gain in the range of 48.25 KHz to 52.25 KHz together with a gradual attenuation at other frequencies are used to supply the currents to the ADC. This attenuation reaches 80 dB at higher frequencies around 105 KHz and also at lower frequencies near 0Hz. The word length of the ADC is chosen to be 12 bits to obtain a Signal to Quantization Noise Ratio (SQNR) of 72 dB so that the quantization noise does not deteriorate the input SNR, which is around 50 dB.

Since all the four PSD currents are similar in terms of frequency components, the beacon channel separation and demodulation methods are common to all of them. Bandpass filtering for the selection of the beacon channel and then envelope detection consisting of rectification and lowpass filtering are performed. Since the beacon carrier frequencies are separated by 500 Hz, the bandpass filter is designed to have a unity gain passband from $f_j - 100$ to $f_j + 100$ Hz, a transition bandwidth of 150 Hz from $f_j - 250$ to $f_j - 100$ and from $f_j + 100$ to $f_j + 250$. The stopband attenuation is around 80 dB. Using the Remez formula [12], a Finite Impulse Response (FIR) filter of the order 3000 is required. There are four PSD currents and each current has eight separate components due to eight different beacons. Implementing 32(=8 beacons *4 PSD currents) FIR filters of order 3000 at a sampling frequency of 210 KHz is not practical on current DSP processors. The number of operations (multiply and accumulate) and memory accesses per sample are directly proportional to the filter order. Therefore, simple envelope detection in the digital domain at higher sampling frequencies for multiple channels is not realizable from a practical standpoint. Furthermore, it should be realized that such a filter is not realizable in the analog domain either since an impractical number of poles are needed. Although the situation can be improved slightly by increasing the separation between the beacon carriers, this increases the maximum frequency of the system and the sampling frequency requirements. In addition, there exist bounds for the modulation process (at around 40 KHz and 100 KHz based on the sensor requirements) as described in sub section B of

this Section II and one may want to deploy up to 24 beacons to improve the redundancy of the system.

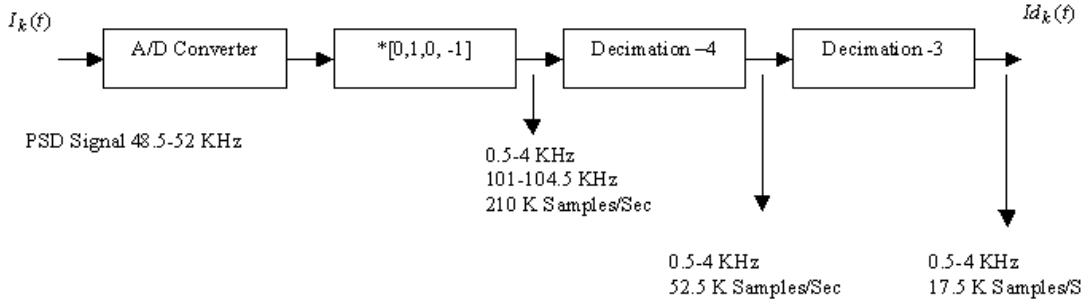

Fig. 6. Heterodyning and down conversion of the composite signal from a PSD terminal

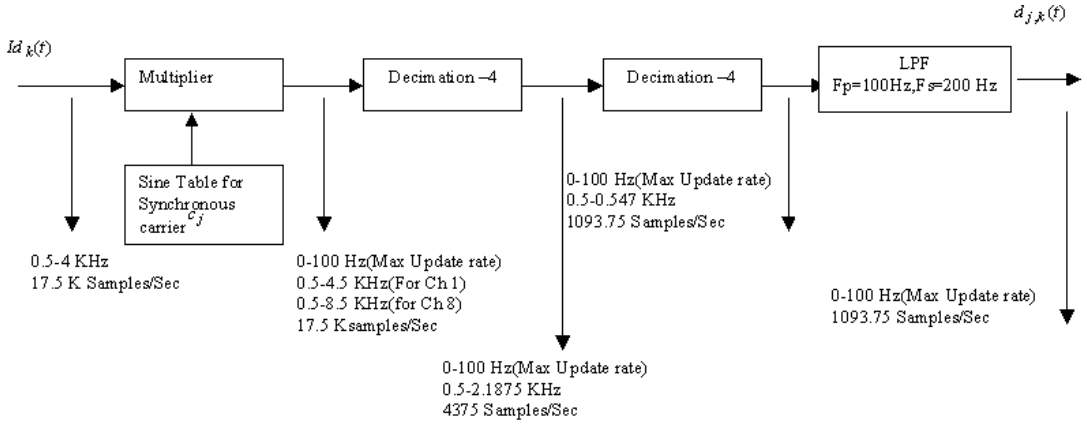

Fig. 7. Synchronous detection for getting PSD response due to a single beacon channel after heterodyning and down conversion of the composite signal from a PSD terminal.

The demodulated currents are communicated from the C55x DSP to the VC33 DSP for navigation solution using the GLSDC algorithm.

Another alternative is to multiply the PSD sensor current with a synchronous carrier. This demodulates the components corresponding to the beacon from the higher frequency range ($f_j - 100$ to $f_j + 100$) to a lower frequency range (0 to 100 Hz). With this approach, it is no longer required to do bandpass filtering to separate the beacon channels since multiplying the composite PSD signal with the required beacon carrier incorporates this separation. This operation involves only one multiplication per sample (multiplication of sine carrier coefficient with the sample) and three memory accesses per sample (reading of sample, reading of sine coefficient from a circular buffer and writing the product into memory). Computationally this is very efficient as compared to the bandpass filtering approach. Note that the local digital oscillator's carrier must be in synchronization with the beacon carrier both in phase and frequency. The beacons are excited by stable crystal oscillators. Since the configuration of the beacons and the frequencies of the beacons are known in advance, only phase synchronization has to be performed at the beginning of the system operation assuming that there is no significant fading of the channel for an operating range of around 100m between the transmitter and the receiver. After the synchronous multiplication, a lowpass filter of passband 0 to 100 Hz and a transition bandwidth of 100 Hz to 500Hz with a stopband attenuation of 80 dB is utilized. To implement this filter at the sampling frequency of 52.5 KHz, a FIR filter of order of about 1942 is needed.

However, implementing 32 FIR filters of order 1942 at the sampling frequency of 52.5 KHz is not practical. For the signal of interest from 0 to 100Hz, the Nyquist rate is only 200 Hz. By using the multi-rate signal processing techniques discussed in [12], this problem is resolved by implementing a narrowband filter at higher frequencies via a combination of decimation and interpolation. Considering that only low frequency components are needed and there is no need to restore the original sampling rate, such a filter can be achieved by just using decimation. The computational requirements on the anti-aliasing or decimation filter are reduced by breaking the decimation into stages [12]. The decimation is performed in steps of 4,3,4,4 achieving a decimation of 192 and a final sampling frequency of 1093.75 Hz.

Since the PSD signal is a narrowband signal of only 2 KHz spanning from 48.25 KHz to 52.25 KHz, if we heterodyne this signal with 52.5 KHz ($F_s / 4$), the PSD signal is down converted to between 0.25KHz and 4.25 KHz. Consequently, the beacon carriers are down converted to the "beated beacon carriers" 0.5 KHz to 4KHz with a channel separation of 500 Hz . These frequencies can be written as

$$fb_j = j * 500 \, , \; j = 1,..N; \; N = 8 \tag{8}$$

Note that the Nyquist rate for the above signal is only 8.5 KHz. Decimation is applied to remove the higher frequency components and to reduce the sampling rate. The decimation is performed in steps of 4 and 3 achieving a decimation of 12 and sampling frequency fb_s of 17500 Hz, which is approximately 4 times the maximum frequency of the down converted PSD signal, 4.25 KHz. Hence, essentially this

heterodyning and decimation procedure transforms the PSD signal from a higher sampling rate of 210 KHz to a lower sampling rate of 17.5 KHz.

Next we proceed with the synchronous detection or envelope detection on the composite signal. However, as explained previously, synchronous detection is computationally more efficient as compared with the bandpass filtering and envelope detection. For the synchronous detection, it is required to multiply the composite PSD signal with carriers fb_j's between 0.5 KHz and 4 KHz with an increment of 500 Hz instead of the carriers f_j's between 48.5 KHz and 52 KHz with an increment of 500 Hz. Synchronous detection requires one to know the value of the carrier sinusoid corresponding to the composite signal. Although this can be calculated by using trigonometric functions, for real-time implementation it is not practical. Instead, a full cycle of the sampled sinusoids at the least common multiple of sampling frequency, i.e. 17.5 KHz, and the frequency of the "beated beacon carrier " are stored. The number of sine values, Ne, to store for the synchronous detection of a carrier f_c at a sampling frequency f_s, if both f_c and f_s are integers, is given by

$$Ne = lcm(f_{c,} f_s) / f_c$$

For the synchronous detection after heterodyning for the carriers fb_j, $j = 1,.., N; N = 8$, the following total number of entries is needed

$$Ne_{total} = \sum_{j=1}^{N} lcm(fb_j, fb_s) / fb_j \qquad (9)$$

From (8) and $fb_s = 17500Hz$, we get a value of 222 for Ne_{total}. If the q-15 integer format representation [13] is used to represent these values, 444 (=222*2) bytes of memory is needed. This storage requirement is easily achieved using the on-chip DSP memory. On the other hand, the synchronous detection approach for the carriers f_j, $j = 1,..,N; N = 8$, at a sampling frequency of $f_s = 210000\ Hz$ requires $Ne_{total} = 1626$ and 3252(=1626*2) bytes of memory for the q-15 integer format representation.

After the multiplication with different beat carriers to get different channels, each channel current is lowpass filtered using the decimation technique. The output SNR for the demodulation system is derived easily by noting that the noise performance of the demodulation is mainly determined by the lowpass filter following the demodulator. Heterodyning mixes the noise band into the band of interest decreasing the SNR by a factor of 2. Table 1 provides a comparison of the computational requirements and tradeoffs for different demodulation schemes and shows that heterodyning with synchronous detection is the best choice.

As previously explained, for the test configuration of 8 beacons, the beacon carrier frequencies start from 48.5Khz with an inter channel separation of 500 Hz. In other words, the beacon carriers are 48.5 KHz, 49.0 KHz, 49.5 KHz, 50.0KHz, 50.5 KHz, 51.0 KHz, 51.5Khz and 52.0 KHz. Since the sampling frequency f_s is selected to be 210 KHz, the beacon carriers can be written as

$$f_j = f_s / 4 - j * 500 \tag{10}$$

As a result, the PSD sensor current at the k^{th} terminal can be written as

$$I_k(t) = \sum_{j=1}^{N} (A_{j,k}.Cos(2.pi.(f_s/4 - j*500).t).(1 + m_{j,k}(t))) + n_{j,k} \tag{11}$$

By heterodyning with a carrier of frequency equal to one fourth of the sampling frequency, i.e.

$c_h = Cos(2.pi.f_s/4.t)$,

the product signal can be written as

$$Ih_k(t) = I_k(t) * c_h$$

$$Ih_k(t) = \sum_{j=1}^{N} \frac{1}{2} (A_{j,k}.Cos(2.pi.(j*500).t).(1 + m_{j,k}(t))) +$$

$$\sum_{j=1}^{N} \frac{1}{2} (A_{j,k}.Cos(2.pi.(f_s/2 - j*500).t).(1 + m_{j,k}(t))) + n_{j,k} \tag{12}$$

Due to heterodyning, the PSD signal gets shifted to low frequencies around 500 Hz and also to high frequencies around $f_s/2$. Now decimation is used to remove the high frequency components and to reduce the sampling rate. Note that heterodyning splits the signal power into two components and causes no difference in the spectral density of white noise. Since only one component is taken, the effective signal spectral density to the noise spectral density in the band of interest is decreased by a factor of 2, or 3 dB deterioration. This is considered to be minimal as the final SNR is around 77dB. Heterodyning with $f_s/4$ is deliberately chosen to reduce the computational

load. Multiplying a signal sampled at f_s with a sinusoid $f_s/4$ involves multiplication with a circular sequence of (0,1,0, -1). Hence, the alternate samples can be ignored and the only operations involved are one sign reversal for every four samples and two memory accesses (refer to Fig. 6).

After the decimation by a factor of 12 in steps of 4 and 3, we will get the following signal sampled at 17.5 KHz:

$$Id_k(t) = \sum_{j=1}^{N} (\frac{1}{2}(A_{j,k}.Cos(2.pi.(j*500).t).(1+m_{j,k}(t))) + nd_{j,k}), \quad (13)$$

The power spectrum for $nd_{j,k}$ is equal to the power spectral density of the output of the lowpass filter for the input $n_{j,k}$ and the impulse response is the convolution of $h1(t)$ and $h2(t)$, where $h1(t)$ and $h2(t)$ are the impulse responses of the lowpass filters for the decimation 4 and 3, respectively. Consequently, noise is filtered out and the SNR improves. The transition band for these decimation filters start from $N*500+100Hz$, thus relaxing the requirements on these filters. This generates some attenuation for the unwanted signal above $N*500+100Hz$.

Now to get the PSD response due to the j^{th} beacon, the above composite signal is mixed with the carrier as shown below:

$$c_j = Cos(2.pi.(j*500).t) \quad (14)$$

$$Id_{j,k}(t) = Id_k(t)*c_j \quad (15)$$

$$Id_{j,k}(t) = \frac{1}{2}.A_{j,k}(1+m_{j,k}(t)) + \sum_{\substack{l=1 \\ l\neq j}}^{N} \frac{1}{4}(A_{l,k}.Cos(2.pi.((l-j)*500).t).(1+m_{l,k}(t))) + \sum_{l=1}^{N} \frac{1}{4}(A_{l,k}.Cos(2.pi.((l+j)*500).t).(1+m_{l,k}(t))) + nd_{l,k} \quad (16)$$

It is required to get the first term in the above equation and to get rid of the high frequency terms. A lowpass filter with the passband from 0 to 100 Hz, transition band from 100 to 200 Hz, stopband from 200 Hz to 17500 Hz is used for this purpose. The stopband attenuation should be around 80 dB. The sampling frequency is 17500 Hz. To minimize the computational requirements, this filter is implemented using the decimation technique. Since the maximum frequency of the first term in (16) is around 100 Hz, a Nyquist rate of 200 Hz is needed assuming no high frequency components. So given the reduction in the high frequency components and sampling rate, such a lowpass filter is readily realized. Decimation of 16 in steps of 4 and 4 is performed on $Id_{j,k}(t)$. This process removes many of the higher frequency terms in (16) giving a sampling frequency of 1093.75 Hz (=17500/16 Hz). The transition band for these decimation filters start from 100 Hz, again relaxing the requirements on these filters. The signals after the decimation and filtering contain the first term and few high frequency components from (16) and can be written as

$$Idd_{j,k}(t) = \frac{1}{2}.A_{j,k}(1+m_{j,k}(t)) + \sum_{\substack{l=j-1 \\ l\neq j}}^{j+1} \frac{1}{4}(A_{l,k}.Cos(2.pi.((l-j)*500).t).(1+m_{l,k}(t))) +$$

$$\sum_{l=j-1}^{j+1} ndd_{l,k} \qquad if \qquad j \neq 1$$

$$Idd_{j,k}(t) = \frac{1}{2}.A_{j,k}(1+m_{j,k}(t)) + \frac{1}{4}(A_{j+1,k}.Cos(2.pi.(500).t).(1+m_{j+1,k}(t))) + \sum_{l=j}^{j+1} ndd_{l,k}$$

$$if \qquad j=1 \quad (17)$$

The power spectral density for $ndd_{j,k}$ is equal to the power spectral density of the lowpass filtering output for the input $nd_{j,k}$ and the impulse response is the convolution of $h3(t)$ and $h4(t)$, where $h3(t)$ and $h4(t)$ are the impulse responses of the lowpass filters for the decimation 4 and 4, respectively, used in the above formulation. Here the noise is also filtered out improving the SNR.

As a result, the required lowpass filter is implemented using the new sampling frequency of 1093.75 Hz with a FIR filter of order 50. The output of the lowpass filter is given by

$$d_{j,k}(t) = \frac{1}{2}.A_{j,k}(1+m_{j,k}(t)) + ndf_{j,k} \qquad (18)$$

The power spectrum for $ndf_{j,k}$ is equal to the power spectral density of the output of the above lowpass filter for the input $nd_{j,k}$. The demodulated current is similar to (5) except for a scaling factor and noise in the passband of the filter, see Fig. 7 on p.18.

III. SIX DEGREES OF FREEDOM DATA ESTIMATION

The normalized voltages computed from the PSD imbalance currents using (6) and (7) due to the i^{th} target are mapped to the horizontal and vertical displacement (y_i, z_i) estimates of that target beacon's image with respect to the sensor frame (see Fig.4 on p.8). This mapping compensates primarily for lens distortion using Chebyshev polynomials [1,15,16,17].

As indicated in Fig.4, V_y , V_z are the normalized voltages; X_i, Y_i, Z_i are the known object space coordinates of the target light source (i^{th} beacon); X_c, Y_c, Z_c are the unknown object space coordinates of the sensor attached to the chase frame; C is the unknown direction cosine matrix of the image space coordinate frame with respect to the object space coordinate frame; F_y , F_z are the lens calibration maps; f is the focal length of the sensor lens and y_i, z_i are the ideal image spot centroid coordinates in the image space coordinate frame corresponding to the i^{th} target light source .

A. System Equations

The sensor electronics, the ambient light sources, and the inherent properties of the sensor produce noise in the PSD measurements. This noise is considered to be zero mean Gaussian noise. The measurement model $\underline{h}_i(\underline{x})$ is given by

$$\underline{h}_i(\underline{x}) = \underline{\tilde{h}}_i(\underline{x}) + \underline{v}_i, \tag{19}$$

where $\underline{x} = [\underline{L} : \underline{O}]^T$ denotes the state vector of the sensor, and $\underline{L} = [X_c \; Y_c \; Z_c \;]^T$ is the position vector, $\underline{O}$ is the orientation vector, which depends on the attitude parameters used, and $\underline{\tilde{h}}_i(\underline{x})$ is an ideal measurement model and is a function of $y_i(\underline{x})$ and $z_i(\underline{x})$,

$$\underline{\tilde{h}}_i(\underline{x}) = F(y_i(\underline{x}), z_i(\underline{x})), \tag{20}$$

and $\underline{v}_i$ is the Gaussian measurement noise with covariance

$$R_i = E\{\underline{v}_i \underline{v}_i^T\} \tag{21}$$

Using the Gaussian Least Squares Differential Correction (GLSDC) algorithm to determine the states, attitude and position, the best geometric solution in the least square sense is obtained upon convergence through iterations [1]. Estimates for position and attitude are refined through iterations of GLSDC as it minimizes the weighted sum of squares given by

$$J = \frac{1}{2}(h - \tilde{h})^T W (h - \tilde{h}), \tag{22}$$

where W is the weighting matrix and

$$W_{i,j} = 1/R_{i,j} = E\{\underline{v}_i \underline{v}_j^T\}. \tag{23}$$

From the geometric colinearity equations, the ideal image centroid coordinates can be written as [1]:

$$
\begin{aligned}
z_i &= g_{zi}(X_i, Y_i, Z_i, X_c, Y_c, Z_c, C) \\
&= -f\,\frac{C_{31}(X_i - X_c) + C_{32}(Y_i - Y_c) + C_{33}(Z_i - Z_c)}{C_{11}(X_i - X_c) + C_{12}(Y_i - Y_c) + C_{13}(Z_i - Z_c)}. \\
y_i &= g_{yi}(X_i, Y_i, Z_i, X_c, Y_c, Z_c, C) \\
&= -f\,\frac{C_{21}(X_i - X_c) + C_{22}(Y_i - Y_c) + C_{23}(Z_i - Z_c)}{C_{11}(X_i - X_c) + C_{12}(Y_i - Y_c) + C_{13}(Z_i - Z_c)},
\end{aligned} \tag{24}
$$

An alternate representation for the above equations can be written based on the unit line of sight vector as [9]

$$\underline{b}_{i3} = C \;\; \underline{r}_i, \tag{25}$$

where

$$\underline{b}_{i3} = (1/\sqrt{f^2 + y_i^2 + z_i^2}).[-f \;\; y_i \;\; z_i]^T \tag{26}$$

are the sensor frame unit vectors,

$$\underline{r}_i = (1/d_i).[(X_i - X_c)\;(Y_i - Y_c)\;(X_i - X_c)]^T \tag{27}$$

are the object frame unit vectors, and

$$d_i = \sqrt{(X_i - X_c)^2 + (Y_i - Y_c)^2 + (Z_i - Z_c)^2} \tag{28}$$

We have choices to make in the coordinate representation for the directional cosine matrix *C* in terms of different attitude representations such as Euler's angles and Modified Rodrigues Parameters (MRP). MRPs are derived from the quaternions and yield better results in terms of linearity since they linearize like quarter-angles instead of half-angles for the quaternions, the interested reader is referred to [18] for more details.

The modified Rodrigues Parameters are defined as:

$$\underline{p} = \underline{e} \tan(\frac{\Phi}{4}) \ , \tag{29}$$

where $\underline{e} = [e_1 \ e_2 \ e_3 \ ]^T$ is the rotation axis; Φ is the principal rotation angle. The 3×3 direction cosine matrix in terms of Modified Rodrigues Parameters is given by [18]

$$C = I_{3\times 3} + \frac{8(\underline{p}\times)^2 - 4(1 - \underline{p}^T \underline{p})(\underline{p}\times)}{(1 + \underline{p}^T \underline{p})^2}, \tag{30}$$

$$\text{and } \underline{p}\times = \begin{bmatrix} 0 & -p_3 & p_2 \\ p_3 & 0 & -p_1 \\ -p_2 & p_1 & 0 \end{bmatrix}. \tag{31}$$

B. Measurement Models

We can now use the y_i, z_i parameters in (24), or the normalized parameters in (26), as the parameters of the measurement model in (19). Here these two models are referred to for convenience as MRP-B2 and MRP-B3, respectively. Since f is constant, there is no need to consider this parameter and this will eliminate the redundancy in calculations. Most of the redundancy is eliminated due to the fact that now the measurement sensitivity matrix H in (40) is $2N \times 6$ instead of $3N \times 6$ and the matrix W in (22) is $2N \times 2N$ instead of $3N \times 3N$.

The simulations have shown that the model MRP-B2 generates less accurate results as the parameter f provides important information when the sensor is very near the target though it achieves computational savings of up to 20% as compared to the model MRP-B3n. A new measurement model is thus presented here, referred to as MRP-B2n, which uses only two parameters with normalization to get better convergence results. That is,

$$\underline{h}_i = (1/\sqrt{f^2 + y_i^2 + z_i^2})[y_i \; z_i]^T, \tag{32}$$

which can be represented as follows

$$\underline{h}_i(\underline{x}) = D \; \underline{r}_i, \tag{33}$$

where $D_{j,k} = C_{j+1,k}$, $j = 1,2; k = 1,2,3$ (34)

This new model MRP-B2n achieves the same convergence results as the MRP-B3n while achieving computational savings of up to 20% as compared to the MRP-B3n. The measurement sensitivity matrix for the i^{th} beacon H_i is obtained by partial differentiation of the measurement model with respect to the state vector $\underline{x}$,

$$H_i = \frac{\partial \underline{h}_i}{\partial \underline{x}} = \left[\frac{\partial \underline{h}_i}{\partial \underline{L}} \;\; \frac{\partial \underline{h}_i}{\partial \underline{O}} \right], \tag{35}$$

$$\frac{\partial \underline{h}_i}{\partial \underline{L}} = -D\{I_{3\times 3} - \underline{r}_i \underline{r}_i^T\} / d_i,$$

and

$$\frac{\partial \underline{h}_i}{\partial \underline{O}} = \frac{4}{(1+\underline{p}^T \underline{p})^2}[S]\{(1-\underline{p}^T \underline{p})I_{3\times 3} - 2[\underline{p}\times] + 2\underline{p}\underline{p}^T\} \tag{36}$$

$$\text{where } S = \begin{bmatrix} s_3 & 0 & -s_1 \\ -s_2 & s_1 & 0 \end{bmatrix}, \underline{s} = [s_1\ s_2\ s_3\ ]^T = C\ r_i \tag{37}$$

The actual measurement matrix for N beacons using (15) is

$$b = [\underline{h}_1{}^T \quad ... \quad \underline{h}_N{}^T\ ]^T . \tag{38}$$

The estimated ideal measurement matrix using estimated position and orientation in the colinearity equation (16) is thus

$$\tilde{\underline{b}} = [\tilde{\underline{h}}_1{}^T \quad ... \quad \tilde{\underline{h}}_N{}^T\ ]^T , \tag{39}$$

and the measurement sensitivity matrix is

$$H = [H_1{}^T; H_2{}^T; ...H_N{}^T\ ]^T . \tag{40}$$

C. Modified GLSDC Algorithm

The initial state $\hat{\underline{x}}_{k,0} = \hat{\underline{x}}_{k-1}$. If $k = 0$, then $\hat{\underline{x}}_{k,0}$ is guessed. Next iterate using the following procedure where $P_{k,i}$ is the covariance and $H_{k,i} = H$ in (22) for the i^{th} iteration at the k^{th} time step; $W_k = W$ in (22), $\underline{b}_k = \underline{b}$ in (38) and $\tilde{\underline{b}}_k = \tilde{\underline{b}}$ in (39) at the k^{th} time step ,

$$\begin{aligned} P_{k,i} &= (H_{k,i}^T W_k H_{k,i})^{-1} \\ \Delta\hat{\underline{x}}_{k,i} &= P_{k,i} H_{k,i}^T W_k (\underline{b}_k - \tilde{\underline{b}}_{k,i}) \\ \hat{\underline{x}}_{k,i+1} &= \hat{\underline{x}}_{k,i} + \Delta\hat{\underline{x}}_{k,i}. \end{aligned} \tag{41}$$

Stop iterating when one of these conditions is met:

1. The states are no longer improved.

2. The number of iterations reaches a specified limit.

This version of GLSDC algorithm is robust when there are four or more beacons measured except near certain geometric conditions that are rarely encountered. An extended Kalman filter can be applied to smooth out these 6DOF estimates and to get the velocities and accelerations of the sensor. The combination of this GLSDC algorithm and a Kalman filter to get the complete navigation solution is more robust than a sequential estimation process using a Kalman filter or a predictive filter for different initial errors and different geometric conditions.

D. Considerations for Frequency Division Multiplexing (FDM)

If the beacons are operated sequentially, the beacon measurements can be modeled as

$$\underline{h}_i(\underline{x}) = D\underline{r}_i + e_i, \tag{42}$$

where $e_i = H_i \Delta x_i$ (43)

and Δx_i is the change in position and orientation from the ideal position and orientation, respectively, due to the sensor relative movement that may have occurred while taking the i^{th} beacon measurements. If FDM is used for the beacons, the error e, which is significant if the sensor relative velocity is greater than 10m/sec, can be eliminated from the beacon measurements. In the case of TDM, the lowpass filter after the demodulation needs to have a passband of about $N \times 100Hz$ (100 Hz is the 6DOF data update rate), whereas in FDM, it needs to have only $100Hz$ and this results in an N factor improvement in the SNR for the demodulated beacon currents in (18). To

achieve the same N factor improvement in the SNR for the TDM mode, the peak power of the LED beacons has to be increased by N so that it consumes the same average power as in the FDM mode. However, this may not be a viable solution since as a result a large number of LEDs is required due to the increased peak power requirements. The N factor improvement in signal to noise power of demodulated beacon currents is the same as a $\sqrt{N}$ factor improvement in signal to noise amplitude ratio (denoted by $SNRa$) for demodulated beacon currents. If we assume that all the beacons have the same $SNRa$, then the diagonal elements in the weighting matrix in (22,23), i.e. $W_{i,i}$s, will be $SNRa$. If we assume no cross correlation between noise sources for different beacons, then all the diagonal elements in the weighting matrix will be zero. The 1-sigma outliers for 6DOF data estimates using GLSDC depends on the covariance matrix P and is given by

$$s1_l = \sqrt{B_{l,l}} / SNRa , \tag{44}$$

where $B = P^{-1}$ which is a nonlinear function of the system in (41), $l = 1,2,..,6$ and $s1_l$ gives the 3-sigma outlier for the 6DOF data $\underline{x}(l)$. So a $\sqrt{N}$ factor improvement in $SNRa$ reduces the final 6DOF data estimate errors by nearly an order of $\sqrt{N}$. For very low $SNRa$s, the non-linearity of the system is going to dominate and little reduction in errors is observed with the increase in $SNRa$. For the TDM configuration, $SNRa$ is in the high range of 2000 at a sensor to beacon distance of 25m so the FDM configuration

has a $SNRa$ of around 5650. This leads to a reduction of 1-sigma outliers and 6DOF estimate errors by a factor of around 2.8 if the number of beacons N is 8.

IV. DSP IMPLEMENTATION AND RESULTS

A. Hardware Description

The channel separation and demodulation algorithms can be implemented on a DSP, an FPGA, or an ASIC. The choice depends on several factors including sampling frequency, computational requirements, amount of parallelism in the algorithm, programmability, power consumption, design time and non-recurring costs. We chose a DSP implementation to gain system flexibility. Given the computational and power requirements, we selected the low power 16-bit fixed-point DSP TMS320C55 manufactured by Texas Instruments. The TMS320C55 architecture is widely used in portable communication devices such as cellular phones.

The TMS320C55 architecture consists of a 16-bit fixed-point data computation unit, an address data flow unit, a program flow unit, and an instruction buffer unit. The processor includes four 40-bit accumulators, four 16-bit data registers, and eight 16-bit auxiliary registers. The fixed-point data path contains five main execution units: a 40-bit ALU, a 16-bit ALU, a 40-bit barrel shifter, and two 17x17-bit multiply-accumulate units. The 40-bit ALU supports dual parallel additions and subtractions by treating 32-bit memory operands as packed 16-bit data. It also supports dual 16-bit maximum and minimum operations. The instructions are variable byte lengths ranging in size from 8 bits to 48 bits for improved code density. The instruction set also includes syntax that allows the programmer or compiler to schedule multiple instructions for parallel

execution. The power consumption is as low as 0.05 mW per MIPS and supports 400 MIPS at an operating clock of 200 MHz [2], [14].

In the VISNAV sensor system, a four-channel synchronous A/D converter operating at 210 KHz supplies the four currents from the preamplifiers, which follow the PSD sensor. These samples are transferred to the internal DSP memory using the Direct Memory Access (DMA) transfer mode of the DSP. The algorithms are programmed in the C55x assembly for the optimal use of the DSP architecture. The method of heterodyning and synchronous detection on a TMS320C55x takes around 20% of the CPU time for eight beacons. The DSP allows up to 16 beacons to be accommodated. A comparison with the other methods is provided in Table 2 on p.42.
The TMS320C55 DSP communicates the demodulated beacon currents to a floating point DSP TMS320VC33 for a subsequent navigation solution. The TMS320VC33 supports 75MIPS and 150 MFLOPS at an operating clock of 150 MHz and consumes less than 200mW per 150 MFLOP [2]. The TMS320C3x is targeted at digital audio, data communications, and industrial automation and control. The TMS320VC33 architecture features two- and three-operand instructions, parallel Arithmetic/Logic Unit (ALU) and multiplier execution in a single cycle, block-repeat capability, zero-overhead loops with single-cycle branches,conditional calls and returns and interlocked instructions for multiprocessing support. It has a register file containing eight 40-bit "extended-precision" registers. The multiplier can multiply 32-bit floating-point input data to produce a 40-bit floating-point result, or 24-bit signed integer input data to

produce a result from which the least-significant 32 bits are retained. The ALU operates on 32-bit signed integer and 40-bit floating-point data, providing arithmetic and logical operations as well as integer/floating-point conversions. The barrel shifter is coupled to the ALU and can perform shifts of up to 32 bits left or right. All multiplies, ALU operations, and shifts have a single cycle latency. Some operations may be performed in parallel; for example, a floating-point multiply and a floating-point add can be performed in the same instruction cycle, and may be used for single-cycle multiply-accumulate. IEEE floating-point formats are not supported. The TMS320VC33 uses an internal 40-bit extended-precision floating-point representation, and uses a 32-bit single-precision floating-point representation when loading or storing floating-point data to memory.The memory architecture is modified harvard and it can support one instruction fetch and two data operand fetches. The memory space is unified and the programmer has the control and flexibilty to map the memory depending on the application requirements.The onchip memory is total 34 KB divided into three blocks of 32 KB,1 KB and 1 KB to support the three simultaneous fetches.For the GLSDC algorithm and associated and control routines, the on chip memory is sufficint to hold the critical program and data.

B. DSP Optimizations

A number of optimizations are performed the assembly code to increase the speed of the algorithms on the DSP. These include the use of repeat block instruction,repeat single instruction,delayed branches and parallel instructions. Many

other optimizations are performed based on the control flow graph of the code. The usefulness of hand optimized assembly can be realized from the observation that around 50% savings are obtained in optimizing the GLSDC routine when compared to a base model of an optimized C with the same memory configuration for the code and data placement. The main reason for the compiler's inabilty to generate inefficient code is that the DSP architectures VC33 and C55 don't have orthogonal instruction set and combined with the fact that the memory structure in a conventional DSP is not easily to understood by the compiler. The programmer has better insight in many cases.

C. Test Setup, Results and Discussion

Different algorithms for channel separation and demodulation as discussed in Section II were implemented on the TMS320C55x DSP processor running at 200 MHz[19,20]. Table 1 provides the comparison of different methods for the demodulation in terms of the theoretical signal to noise ratio, the obtained signal to noise ratio, and the number of clock cycles needed per second. Note that $N_c > 1$ means the processor could not complete the specified algorithm in real-time and required more clock cycles than the available clock cycles.

For testing the 6DOF estimation algorithm[20,21], the VISNAV sensor system was used for navigation during a 100m to zero approach of a vehicle in 50 seconds. Simulations were used for sensor measurements and noise estimates for these measurements were obtained from the calibration and accuracy experiments [1],

Table 1. Demodulation Methods.

Method	SNR_o	SNR_o[1]	N_c for N=8	N_c for N=16
Synchronous Demodulation (SD)	SNR_L	79.9	0.6	>1
Heterodyning & SD	$SNR_L/2$	77.0	0.2	0.5
Envelope Demodulation (ED)	SNR_L	79.5	>1	>1
Heterodyning & ED	$SNR_L/2$	76.9	0.4	>1

SNR for Ideal Demodulator $SNR_L = SNR_i * f_{MAX} / f_{LPF}$, $f_{MAX} = 105\,KHz$, $f_{LPF} = 100\,Hz$

[1] $SNR_{idB} = 50dB, SNR_{LdB} = 80dB, f_{S_s} = 2 f_{MAX}$

[1] On a $200MHz$ $C55x$,No. of clocks/second $N_{ca} = 200e6$.

N_{cn} = No. of clocks needed/second. $N_c = N_{cn} / N_{ca}$.

N =Number of beacons.

which consisted of the sensor sitting on a yaw-pitch actuator and the beacons on a rectangular optical table. Initially PSD was at the starting point and moved towards the docking point where the beacons were placed, see Fig. 8 on p.43. The simulated VISNAV sensor measurements were calculated from the ideal forward model of the

colinearity equations. Gaussian noise was added to the measurements based on the signal to noise amplitude ratio (*SNRa*) variations, which was a function of the sensor distance to the target (refer Fig.8 on p.43). A constant voltage *SNRa* of 5000 (~74 dB) and a SNR of 225 (~47 dB) for the PSD sensor were considered. Channel separation and demodulation using heterodyning and synchronous detection provided a gain of 27 dB for the outputs generated by the C55x DSP (refer Table 1,Fig.6 and Fig.7 on p.18). For a sensor distance to target beacons greater than 35m, the beacons were assumed to be unable to provide enough power to bring the maximum PSD signal current to 70% of its saturation level. So beyond 35m, the *SNRa* was assumed to vary inversely with the square of the distance.

Figs. 9 and 10 illustrate the variation of position errors and attitude errors as a function of distance along the x- axis for the GLSDC algorithm with the measurement model MRP-2N.The true (X, Y, Z) positions of the sensor relative to the target frame at the start of the trajectory were (-100m, 30m, 10m) and the initial guesses supplied to the GLSDC algorithm were (-1m, 1m, 1m). The true Modified Rodrigues Parameters of the sensor relative to the target frame at the start of the trajectory were (4.7315e-002, -3.9702e-002, 4.7315e-002) and the initial guesses supplied to the GLSDC algorithm were (0,0,0). The standard deviations of the GLSDC estimated data were represented by the envelope lines, lying symmetrically above and below the zero error axis. The x-axis estimate contained the least noise everywhere along the trajectory, its standard deviation being approximately half that of the y-axis and z-axis. This was a

consequence of all the targets lying close to a plane. A similar result was observed for the three spacecraft Euler angles where the roll angle estimate contained the least noise. The position errors at the beginning of the maneuver were around 5m, and reduced to a few millimeters as the vehicle reached its target destination. The attitude errors at the beginning of the maneuver were around 5 degrees, and reduced to 1/100 degree as the vehicle reached its target destination. As illustrated in Fig. 10, the errors reduced gradually as the sensor was approaching rendezvous. The condition number of the P matrix in (22) improved as the sensor approached the target due to a better beacon/sensor geometry as shown in Fig. 11. Fig. 12 shows the plot of the required iterations for the convergence of the GLSDC algorithm for each and every measurement assuming no limit on the iteration limit. The accuracies and convergence results are almost similar to the results obtained by the GLSDC algorithm using the measurement model-3N. Figs. 11,12 and 13 provide a comparison of the MRP-3n and the MRP-2n models. For the simulated trajectory, the average number of iterations for MRP-3n was 1.29 and for MRP-2n was 1.47.

For real-time operation, instead of trying to achieve convergence with one measurement set (the normalized voltages for all the N beacons), we attempted to achieve convergence over a number of measurement sets. The maximum number of iterations for a measurement set on the TMS320VC33 for an eight-beacon configuration with 100 Hz 6DOF data update rate, is set to an integer number greater than or equal to the average number of iterations. So the maximum number of

iterations allowed for one measurement set for both the models MRP-2n and MRP-3n was set to be the same and equal to 2. The 6DOF data estimates from the VC33 were computed using ten measurement sets from the C55x. Each measurement set was available from the C55x at around 1000 Hz (1093.75 Hz). Various estimation algorithms such as the GLSDC with attitude representation in Euler angles [1], called Euler-2 here, and in MRPs were implemented on the floating point DSP TMS320VC33 (VC33).

Table 2: 6DOF Estimation.

GLSDC	Flops	Robustness	VC33 clock cycles*
Euler-2	0.8M	Low	32e3
MRP-3n	M	High	49e3
MRP-2n	0.8M	High	39e3
MRP- 2	0.8M	Low	39e3

*VC33 results for 8-beacon case and a single iteration.

Table 2 provides the comparison of computational requirements and the robustness for the Gaussian Least Squares Differential Correction (GLSDC) algorithms with different measurement models. Here MRP-3n was considered to be the reference frame for the required number of floating point operations (flops). The number of -flops required by Matlab for this algorithm was equal to M . The robustness measure is based on the algorithm lock after applying different guesses for the initial position and attitude estimates at the start of the navigation. The algorithm was implemented on the TMS320VC33 in optimized assembly and the results are shown in Table 2 for the case of eight beacon configuration.

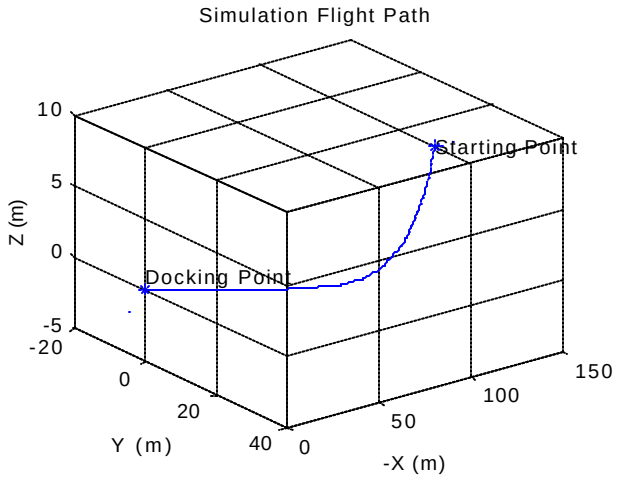

Fig. 8. Simulated flight trajectory.

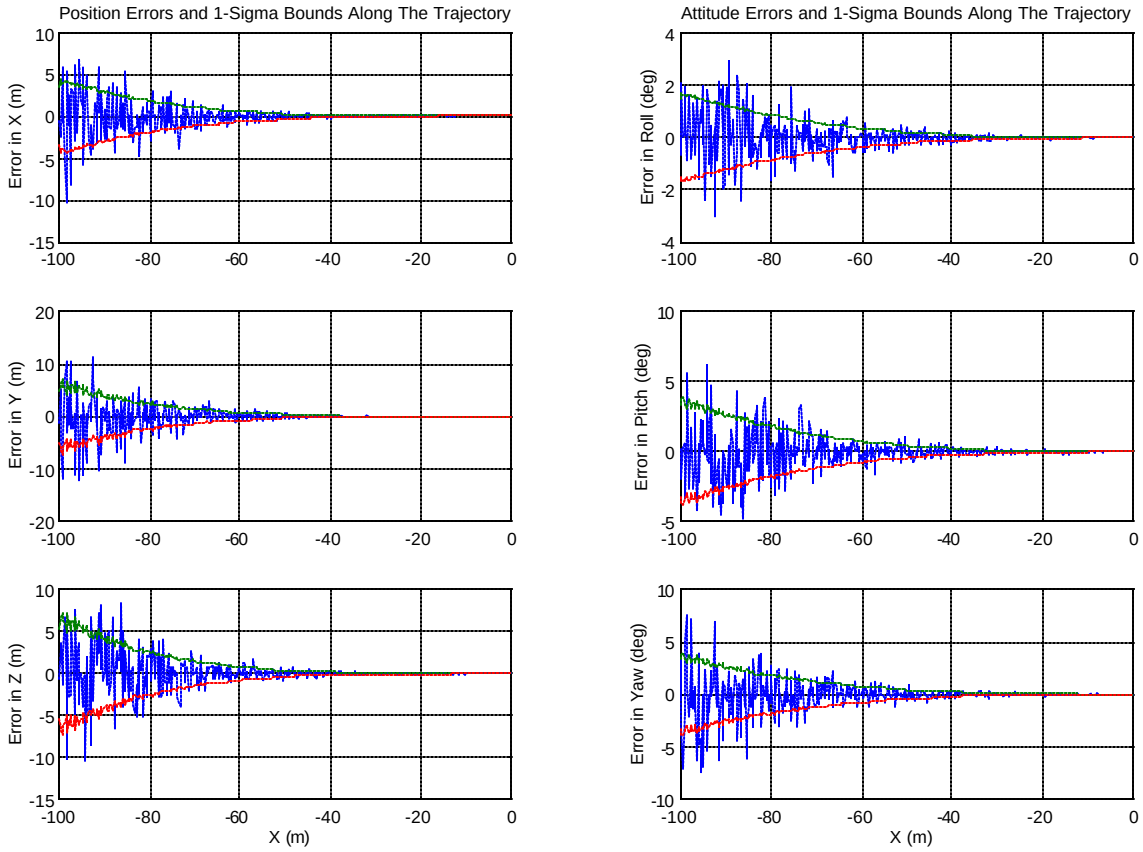

Fig. 9. Position and attitude errors along the trajectory when GLSDC with the measurement model MRP2N is applied to VISNAV sensor measurements.

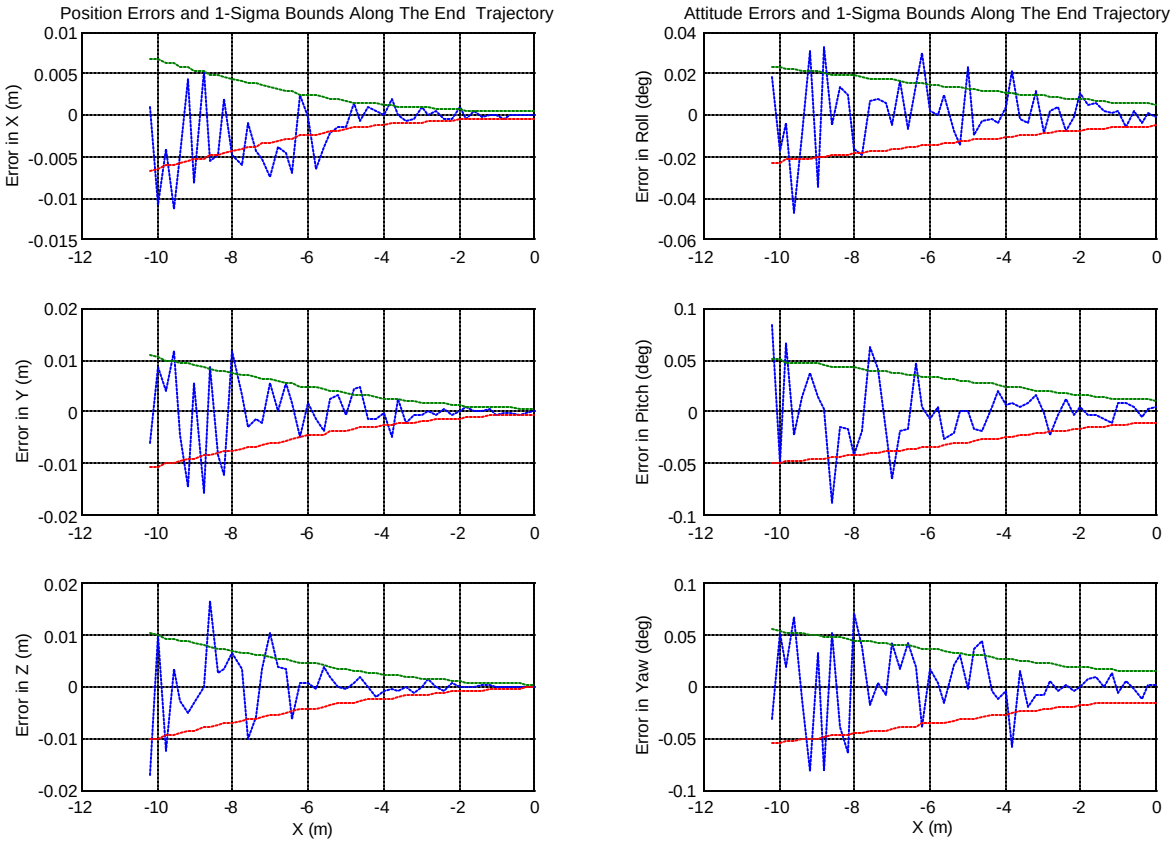

Fig. 10. Position and attitude errors at the rendezvous when GLSDC with the measurement model MRP-2n is applied to VISNAV sensor measurements.

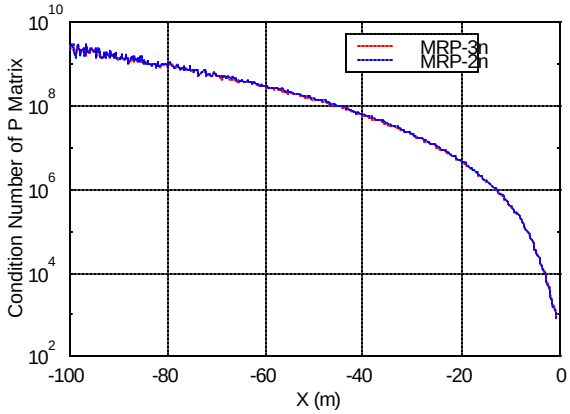

Fig. 11. Condition number of P matrix when the MRP-2n and MRP-3n models are applied to VISNAV sensor measurements.

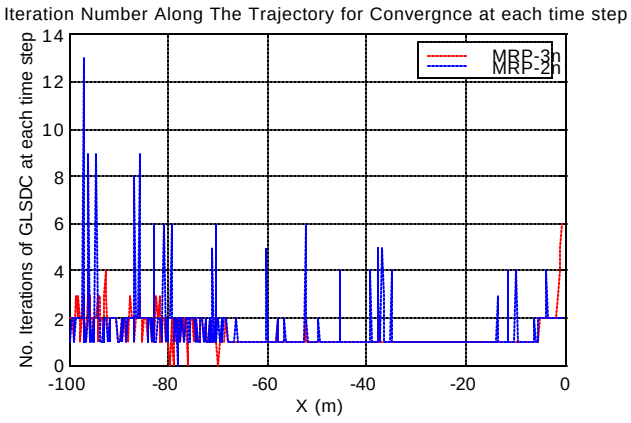

Fig. 12. Comparison of number of iterations taken by MRP-3n and MRP-2n for convergence at each time step.

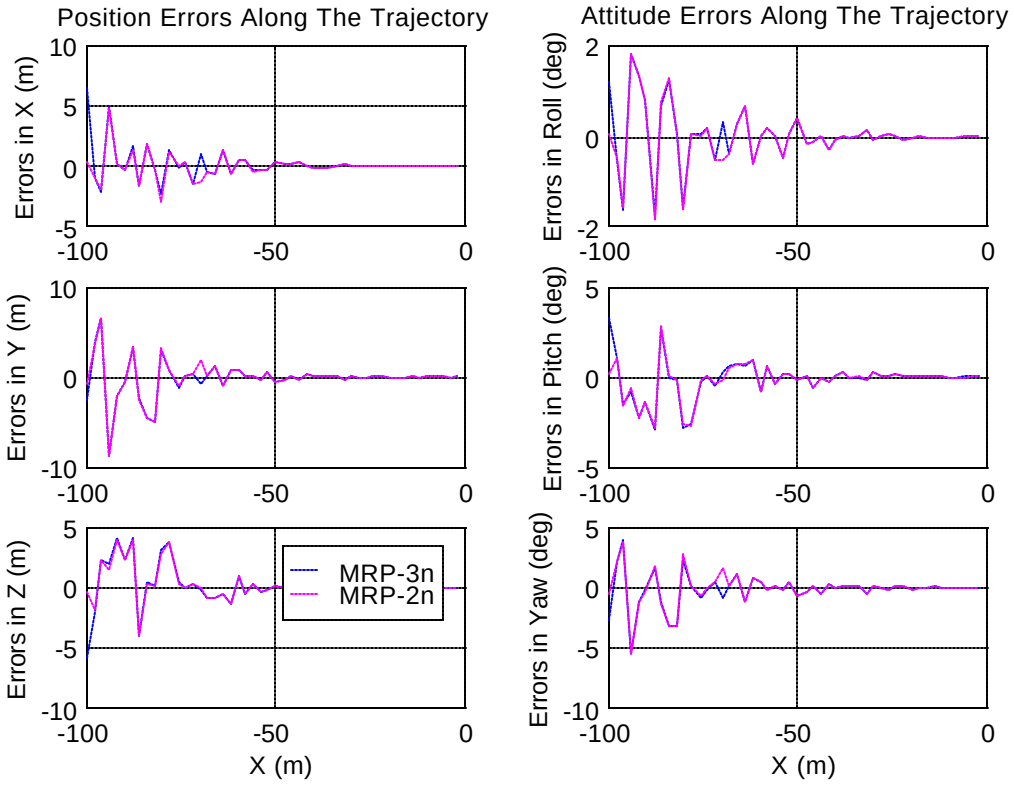

Fig. 13. Comparison of position and attitude errors along the trajectory when GLSDC with the measurement models MRP-2n and MRP-3n are applied to VISNAV sensor measurements.

V. CONCLUSIONS

A new method for operating beacons and demodulating the beacon currents for the VISNAV sensor system is introduced in this paper. It is shown that target differentiation based on frequency division multiplexing yields higher signal to noise ratios for the sensor measurements and the demodulation in the digital domain using multi-rate signal processing techniques brings reliability and flexibility to the sensor system. An optimal associated six degrees of freedom data estimation algorithm using Modified Rodrigues Parameters is presented which is applied to the measurements from the VISNAV sensor to get the navigation solution. This algorithm is robust when there are four or more line of sight measurements except near certain geometric conditions that are rarely encountered. It is shown that this algorithm is computationally efficient and achieves better results than the algorithms that deploy Euler angles for attitude representation.

REFERENCES

[1] J.L.Junkins, D.C.Hughes, K.P.Wazni, and V. Pariyapong, "Vision Based Navigation for Rendezvous, Docking, and Proximity Operations," *Proc. of 22nd Annual AAS Guidance and Control Conference*, AAS 99-021, February 1999.

[2] Information on Texas Instruments Digital Signal Processors (DSP) ,2001 [Online]. Available: http://dspvillage.ti.com/

[3] Information on Global Positioning System, 2001.[Online] Available: www.gpsworld.com

[4] R. Howard, T. Bryan, M. Book, and R.Dabney. "The Video Guidance Sensor-A Flight Proven Technology," *Proc .of 22nd Annual AAS Guidance and Control Conference*, AAS 99-025, February 1999.

[5] P. Calhoun and R.Dabney, "A Solution to the Problem of Determining the Relative 6 DOF State for Spacecraft Automated Rendezvous and Docking," *Proc. of SPIE Space Guidance, Control, and Tracking* II, Orlando, Florida, 17-18 April, 1995.

[6] S.D.Lindell and W.S.Cook, "Closed-loop Autonomous Rendezvous and Capture Demonstration Based on Optical Pattern Recognition," *Proc. of 22nd Annual AAS Guidance and Control Conference*, AAS 99-027, February 1999.

[7] M.Mokuno, I.Kawano and T.Kasai, "Experimental Results of Autonomous Rendezvous Docking on Japanese ETS-VII Satellite," *Proc. of 22nd Annual AAS Guidance and Control Conference*, AAS 99-022, February 1999.

[8] J.L.Junkins, G.Ju, H.Kim and T.Pollock, "Digistar: A Low Cost Micro Star Tracker," *Proc. of AIAA Space Technology Conference and Exposition*, Albuquerque, NM, September 28-30, 1999.

[9] Alonso, R., Du, J.-Y., Hughes, D., Junkins, J.L., and Crassidis, J.L., "Relative Navigation for Formation Flight of Spacecraft," *Proc. of the Flight Mechanics Symposium*, NASA-Goddard Space Flight Center, Greenbelt, MD, June 2001.

[10] J. Valasek, J. Kimmett, D. Hughes, K. Gunnam and J. Junkins, "Vision Based Sensor and Navigation System for Autonomous Aerial Refueling," *Proc. of 1st AIAA Unmanned Aerospace Vehicles, Systems, Technologies, and Operations Conference*, Portsmouth, VA, AIAA-2002-3441, 20-22 May 2002.

[11] Vision Based Navigation System,2001 [Online]. Available: http://jungfrau.tamu.

Edu/~html/VisionLab/

[12] P. P. Vaidyanathan, *Multirate Systems and Filter Banks*, Englewood Cliffs, NJ, Prentice Hall 1993.

[13] N.Kehtarnavaz and M.Keramat *DSP System Design: Using the TMS320C6000*, Englewood Cliffs, NJ, Prentice Hall 2001.

[14] Review of DSP Processors. [Online]. Available:http://www.bdti.com/procsum/tic55xx.htm

[15] Karim P. Wazni, *Vision Based Navigation Using Novel Optical Sensors,* M.S. Thesis, Texas A&M University, College Station,1999

[16] J.L Junkins, D.C.Hughes, H.Schaub, *Non Contact Position and Orientation Measurement System and Method,* US Patent 6,266,142.

[17] Du, J.-Y, *VISNAV System Calibration,* Internal Project Document, VISNAV project, 2002.Contact: Dr. John Junkins . email:junkins@tamu.edu.

[18] J.L. Junkins, *An Introduction to Optimal Estimation of Dynamical Systems,* Alphen Aan Den Rijn, The Netherlands, Sijthoff & Noordhoff International Publishers 1987.

[19] K.Gunnam, D.Hughes, J.Junkins, and N.Kehtarnavaz J.-Y, " A DSP Embedded Optical Navigation System,"*Proceedings of Sixth IEEE International Conference on Siganl Processing,* Beijing, August 2002.

[20] K.Gunnam, D.Hughes, J.Junkins, and N.Kehtarnavaz,"A Vision-Based DSP Embedded Optical Navigation Sensor," *IEEE Sensors Journal,* vol.2, pp. 428-442, October 2002.

[21] J. Valasek, J. Kimmett, D. Hughes, K. Gunnam and J. Junkins, "Vision Based Sensor and Navigation System for Autonomous Aerial Refueling," *AIAA Journal of Guidance, Control and Navigation,*2003.Submitted.

APPENDIX

SENSOR CALIBRATION

We need to map the normalized voltages computed from the PSD imbalance currents due to the i^{th} target are mapped to the horizontal and vertical displacement $(y_{i,} z_i)$ estimates of that target beacon's image with respect to the sensor frame.This mapping is neeeded to compensate primarily for lens aberrations such as spherical aberration, coma,astigmatism,curvature of field and lens distortion. The other sources of error include misalignment of camera assembly, spatiality of optical source and nonlinearity of PSD etc.

The general camera calibration model can be modeled using Chebyshev polynomials [1,15,16,17].

$$\bar{y}_i = F_y(V_y, V_z) = \sum_{i=0}^{n}\sum_{j=0}^{i} a_{ij} f_{ij}(V_y, V_z) = \sum_{i=0}^{n}\sum_{j=0}^{i} a_{ij} T_{i-j}(V_y) T_j(V_z)$$

$$\bar{z}_i = F_z(V_y, V_z) = \sum_{i=0}^{n}\sum_{j=0}^{i} b_{ij} f_{ij}(V_y, V_z) = \sum_{i=0}^{n}\sum_{j=0}^{i} b_{ij} T_{i-j}(V_y) T_j(V_z)$$

Initially a number of Line of sight vector measurements of the sensor $V_{y,}V_z$ by moving the PSD on a yaw-pitch actuator while placing a single beacon in a known position in a noise free and dark room so as to ensure that the distortion present is only

due to lens. Now least squares method is applied to determine the coefficints (a_{ij}, b_{ij}) by having a least sqaures fit of ideal measurements $\bar{y}_i, \bar{z}_i$ (calculated based in the known configuration from the colinearity equations) to the bivariate orthogonal Chebyshev polynomials $f_{ij}(V_y, V_z)$. Because of the orthogonality these polynomials can be represented as single variate Chebyshev polynomials $T_i(V_y)$ and $T_i(V_z)$ of the order n.The order determines the accuracy of the mapping.

Once this calibration procedure is done offline, for the actual operation of the sensor we can use these pre computed coefficients (a_{ij}, b_{ij}) and compute Chebyshev polynomilals as a function of online measurements and correspondingly the horizontal and vertical displacement $(y_{i,} z_i)$ estimates.

VITA

Kiran Kumar Gunnam

Ramalayam St

Peddada

INDIA -533345

Kiran K. Gunnam was born in Peddada, India in 1977. He received the B.Tech Degree in Electronics and Communications Engineering from Jawaharlal Nehru Technological University College of Engineering, Kakinada, India in 1999. He received the Diploma in Electronics and Communications Engineering from Andhra Polytechnic, Kakinada, India in 1995. He is a graduate student in Wireless Communications and Signal Processing program of Department of Electrical Engineering at Texas A&M University, College Station, Texas. His graduate studies and research from January 2000 to May 2002 are funded and guided by Dr. John Junkins and Dr. Nasser Kehtarnavaz as the Co-Chairs of his thesis committee.

He was a graduate research assistant with Dr. Junkins in the Department of Aerospace Engineering, for two years, and in the Department of Electrical Engineering with Dr. Kehtarnavaz for one semester, both times under the supervision and direction of Dr. Declan Hughes. He worked as a Co-op Engineer in Intel Corporation, Santa Clara in Itanium Processor group from May 2002 to November 2002 and then worked for a brief period in Centrino Mobile Processors group. Presently, he is working in Micro Architecture Research, Intel Labs. His research interests include signal processing and computer architecture.